RSC Advances

PAPER

View Article Online
View Journal | View Issue

Cite this: *RSC Adv.*, 2021, **11**, 37760

Hydroxyl ions: flexible tailoring of Cu_2O crystal morphology†

Xiaodong Yang,[ab] Jia Li,[c] Jianhua Yao,*[c] Tianrui Ren *[b] and Bo Zhang*[b]

Received 27th April 2021
Accepted 2nd November 2021

DOI: 10.1039/d1ra03296h

rsc.li/rsc-advances

The precise control architectures of Cu_2O crystals are very crucial, which have a significant influence on their various performances. Herein, Cu_2O crystals with diverse architectures were achieved *via* finely adjusting the concentration of NaOH. The intriguing results showed that the addition of specific amounts of OH^- to the solution was crucial to tailor the morphology and size of the resulting microcrystals. We observed the evolution of the shapes of the Cu_2O microcrystals, which change from a rhombic dodecahedron to spherical, octahedral-like and then to hexapod upon the increase in the NaOH concentration. Adjusting the volume of NaOH added provides a means to vary the particle size. Furthermore, density functional theory (DFT) may reveal that OH^- ions serve as an efficient coordination agent selectively adsorbing onto different crystal faces of Cu_2O crystals modifying the crystal energies, inducing the structure anisotropy on crystal growth. This work reveals that an effective and facile strategy has been developed for morphology-control of Cu_2O crystals.

Introduction

Tailoring the architecture of nano/microcrystals has been of great research interest due to their unique shape and size-dependent properties.[1,2] The shape and size of inorganic materials are well-known to have great effects on their widely varying properties.[3,4] As a p-type semiconductor with direct band-gap of 2.17 eV, cuprous oxide (Cu_2O) is a perspective material,[5] which is widely applied in solar energy conversion,[6] catalysts,[7] gas sensors,[8] templates[9] and antibacterial activity.[10]

Shape-controlled synthesis of Cu_2O crystals has attracted much attention in recent years, and Cu_2O crystals with different morphologies have been successfully synthesized, such as cubes,[11] octahedra,[12] hollow spheres,[13] tetrapods,[14] rhombic dodecahedra,[15] hollow octadecahedra,[16] *etc.* for their specific properties and corresponding potential applications. Furthermore, synthesis of Cu_2O crystals is regulated by various factors, among them, concentration of hydroxyl has been considered as one of the most promising methods for preparing the Cu_2O with various morphologies and size. For example, Yeo *et al.*[17] found the controlled shape evolution of Cu_2O from a cube to a beveled cube and then to a rhombicuboctahedron and a 50-facet polyhedron upon the increase in the NaOH concentration. Similar findings were made by Tang and coworkers[18] who found that interesting morphology-evolution of Cu_2O from initial cubic to final octahedral architectures was readily achieved by adjusting the concentration of hydroxyl. Furthermore, Kuo *et al.*[19] reported that adjustment of the volume of NaOH added provides a means to vary the particle size of octahedral Cu_2O nanocrystals with sizes of 160–460 nm.

Herein, a facile route has been successfully developed for the synthesis of a series of morphologically different Cu_2O crystals. Interestingly, sodium hydroxide can subtly determine the morphology of the final products. Various concentrations of NaOH can result in a series of morphologies of Cu_2O, such as rhombic dodecahedral, spherical, octahedral-like and hexapod architectures. Remarkably, the possible formation mechanism of Cu_2O crystals were investigated using DFT simulation.

Experimental section

Chemicals

Copper(II) chloride dihydrate ($CuCl_2 \cdot 2H_2O$; 99%), hydroxylamine hydrochloride ($NH_2OH \cdot HCl$; 99%), sodium hydroxide (NaOH, 98.2%), and sodium dodecyl sulfate (SDS; 99%) were purchased from Aladdin. All chemicals were used as received without further purification. Ultrapure distilled and deionized water (18.3 MΩ) was used for all solution preparations.

Cu_2O crystals synthesis

The synthesis of various Cu_2O crystals was finely tailored the concentrations of OH^- ions, and the synthesis routes of Cu_2O are presented in Scheme 1. Typically, 100 mL of deionized water,

[a]State Key Laboratory Breeding Base of Green Pesticide and Agricultural Bioengineering/Key Laboratory of Green Pesticide and Agricultural Bioengineering, Ministry of Education, Guizhou University, Guiyang, 550025, P. R. China

[b]Shanghai Engineering Research Center of Green Energy Chemical Engineering, College of Chemistry and Materials Science, Shanghai Normal University, 100 Guilin Road, Shanghai, 200234, P. R. China. E-mail: trren@shnu.edu.cn; zb830216@shnu.edu.cn

[c]CAS Key Laboratory of Energy Regulation Materials, Shanghai Institute of Organic Chemistry, Chinese Academy of Sciences, Shanghai 200032, China. E-mail: yaojh@mail.sioc.ac.cn

† Electronic supplementary information (ESI) available. See DOI: 10.1039/d1ra03296h

7.5 mL of 0.1 M $CuCl_2$ solution and 1.3 g of SDS powder were added into the flask with vigorous magnetic stirring at 30 °C. After complete dissolution of SDS, a serious of 1 M NaOH solution for the desired R (R is defined as the molar ratio of OH^- to Cu^{2+}) was quickly added into the above mixtures under stirring, which resulted in a light blue colored solution containing $Cu(OH)_2$ precipitate. Then, 35 mL of 0.1 M $NH_2OH{\cdot}HCl$ was quickly injected into the mixed solution under vigorous stirring. The mixed solution was adequately stirred for kept 1 h. The resulting precipitate was centrifuged, washed with the distilled water and absolute ethanol, and finally dried at 50 °C for 6 h in vacuum.

Theoretical calculation

The interaction energies between OH^- ions and different facets of Cu_2O crystal were investigated by polymer consistent force filed (PCFF),[20] dynamic simulation in Accelrys Materials Studio.[21]

Instrumentation

Field emission scanning microscopy (FESEM) was taken with Hitachi S-4800 operating at 1.5 kV. UV-vis absorption spectra were acquired by UV-vis spectrophotometer (UV-2000, UNICO (Shanghai) Instruments Co., Ltd.). The X-ray diffraction (XRD) patterns were obtained from a PANalytical X'pert MPD Prodiffractometer operated at 40 kV and 40 mA using Ni-filtered CuK irradiation (wavelength 1.5406 Å). X-ray photoelectron spectroscopy (XPS) spectra were obtained using a PerkinElmer PHI-5000C ESCA system.

Results and discussion

Morphology analysis of Cu_2O crystals *via* tuning the amounts of OH^- ions

The concentration of NaOH as a coordination agent affected the reducing power of the reducing agents and the reaction rate, which can influence the branching growth of Cu_2O. In this article, Cu_2O crystals with various morphologies including rhombic dodecahedra, spherical, octahedron-like and hexapod were achieved by adding 0.750–7.5 mL of 1.0 M NaOH solution and then $NH_2OH{\cdot}HCl$ solution to an aqueous $CuCl_2$ solution at room temperature for 1 h. The morphology and size of particles were achieved by progressively increasing the volume of NaOH solution (see Scheme 1 and Table S1† for the exact reagent amounts used), as shown in Fig. 1–3. Additionally, we examined pH values by adding different concentrations of NaOH (Table S1†).

In the process of solution synthesis, Cu_2O is prepared from the following reaction. Firstly, OH^- ions were added into the Cu(II) solution, $Cu(OH)_2$ was the first to form from the solution (eqn (1)). When the concentration of OH^- ions was high, $[Cu(OH)_4]^{2-}$ complexes would be formed (eqn (2)). Secondly, upon the introduction of $NH_2OH{\cdot}HCl$, Cu_2O was synthesized by the $[Cu(OH)_4]^{2-}$ species (eqn (3)).

$$Cu(II) + 2OH^- \rightarrow Cu(OH)_2 \quad (1)$$

$$Cu(OH)_2 + 2OH^- \rightarrow [Cu(OH)_4]^{2-} \quad (2)$$

$$2[Cu(OH)_4]^{2-} + NH_2OH{\cdot}HCl \rightarrow Cu_2O + N_2 + 4OH^- + H_2O \quad (3)$$

The above reaction suggests that the formation of different Cu_2O crystals may be related to the concentration of hydroxide ions in the solution. When adding different volume of NaOH, the mother solution changes from acidic to alkaline. Thus, the pH-dependent precursors are formed by the changes in pH and allows us to manipulate the reduction kinetics of the crystallization of Cu_2O. Various copper precursors firstly influenced the thermodynamics of the chemical reaction, due to the pH-dependent reduction potentials of the copper precursors. Then, the sizes and morphologies of the final products were influence by the redox and complexation reactions.[22]

When R is 1, no Cu_2O crystals were still produced, probably because of dissolution of the obtained Cu_2O by $NH_2OH{\cdot}HCl$. When R increases to 2 and 3, Fig. 1A and B clearly showed that the obtained samples with exposed 12 well-defined high-energy {110} planes possess perfect and regular rhombic dodecahedral morphology with the average diameters of 0.48 and 0.45 μm, respectively (Fig. S1†). Surprisingly, with R increase to 3.5, uniform octadecahedron Cu_2O crystals (Fig. 1C) were fabricated and had well-defined facets and smooth surfaces with average size of 0.91 μm (Fig. S2c†). Compared to the rhombic dodecahedral Cu_2O crystals, octadecahedron Cu_2O crystals emerged new {100} facets, and had 12 hexagonal {110} facets and 6 square {100} facets, suggesting that the growth rate along the ⟨110⟩ direction exceeds that of ⟨100⟩ direction.[23,24] The above results suggested that a lower pH of solution system (R was 2 or 3, Table S1†) favor the formation of rhombic dodecahedral Cu_2O crystals, that is, the rhombic dodecahedral Cu_2O crystals exposing twelve {110} facets are stable in a lower acid systems, which is in accordance with the literature results.[25,26]

We can interpret the evolution of morphologies of Cu_2O crystals from the atomic level of interactions between OH^- ions

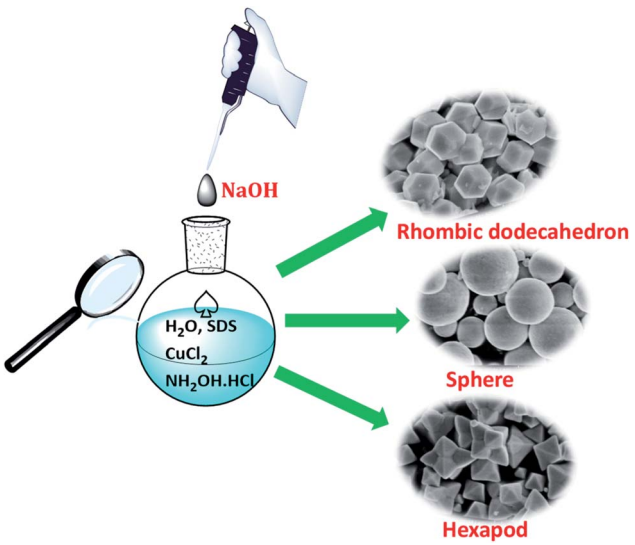

Scheme 1 Schematic illustration of the synthesis processes for Cu_2O crystals with various morphologies.

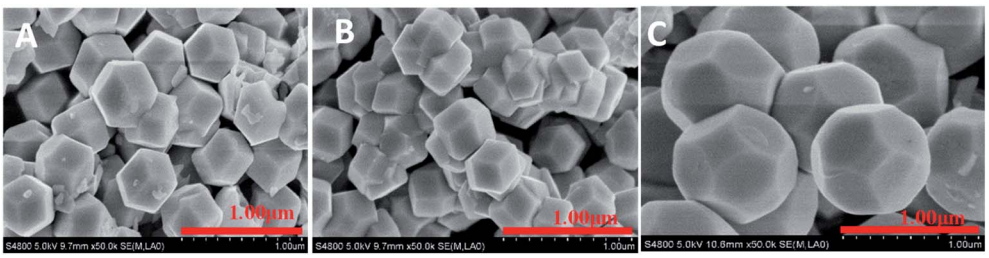

Fig. 1 FESEM images of Cu_2O crystals obtained with different *R*, (A) 2, (B) 3 and (C) 3.5.

and various facets. The evolution of the morphology of the Cu_2O crystal is governed by the continuous decrease in the total surface energy. Fig. 2A illustrates that Cu_2O crystals is a cubic structures, where the 'O' atom is surrounded by a tetrahedron of 'Cu' atom, and each 'Cu' atom has two oxygen atom as neighbors.[26,27] The surface atom arrangements of {100}, {111} and {110} facets are completely different (Fig. 2B–D). {100} facets of Cu_2O are predominated by Cu or O atoms only, leading to the electrically neutral state.[25,28] The {111} and {110} facets are formed with Cu and O atoms and the Cu atoms with dangling bonds which can make them positively charged.[29–31] Consequently, a stronger adsorption between negative OH^- ions and the Cu atoms on the {111} and {110} facets than on the other facets has been indicated.[32,33] Whereas {110} planes have a higher density of Cu dangling bonds than that of the {111} planes. The number of terminal copper atoms per unit surface area on the {110} face is roughly 1.5 times higher than that found on the {111} face. The {110} face is likely more positively charged compared to the {111} facet.[34] Therefore, the relative surface energies of the Cu_2O crystals are in the following order: {110} > {111} > {100}, which leads to higher adsorbing capacity with lower OH^- ions than {111} facet.[17] Such a trend is consistent with that obtained from theoretical calculations. The interaction energies between OH^- ions and different facets of Cu_2O crystal were are summarized in Table 1.

Thus, when *R* were 2 and 3, OH^- ions preferentially adsorbed on the {110} facet, the growth rate along the ⟨111⟩ direction far exceeds that of the ⟨100⟩ direction, the {110} facets finally remained, therefore the RD Cu_2O crystals were formed (Fig. 1A and B). As *R* was increased to 3.5, OH^- ions could be adsorbed on the {111} facets of Cu_2O crystals and slow the growth rates of the {111} facets. However, at this point, surface energy of {100} facet is still less than {111} facet, promoting the appearance of 100 faces. Thus the truncated rhombic dodecahedral structure (octadecahedron) with {100} and {110} facets appeared.

With the further enhancement of *R* to 4, 5 and 6 (Fig. 3A–C), nonuniform spherical Cu_2O products with rough surfaces were fabricated, the as-prepared Cu_2O products were composed of some small particles and many large spherical Cu_2O particles. The shape evolution of Cu_2O presumably through nanoparticle-aggregated spheres was achieved, which is in accordance with the literature.[35]

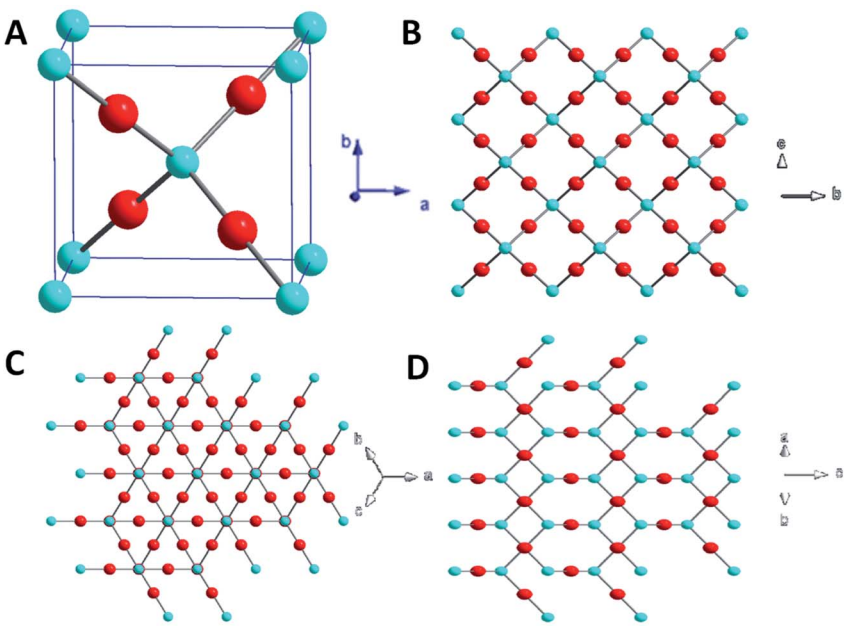

Fig. 2 Copper (Cu) atoms are shown as blue spheres, and oxygen (O) atoms are shown as red spheres. (A) Illustration unit cell of the Cu_2O. The crystal structures of Cu_2O particles with different facets: (B) {100}, (C) {111} and (D) {110} facets, respectively.

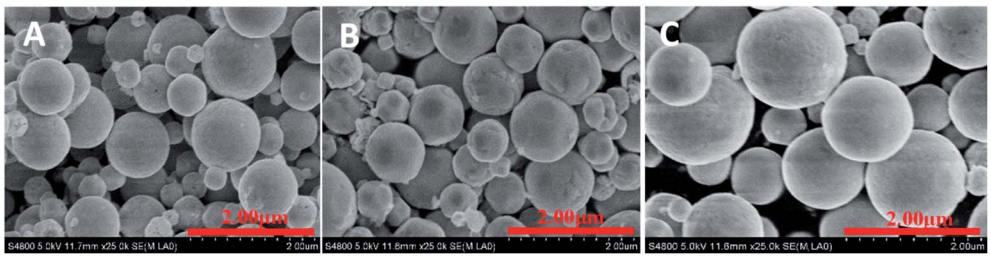

Fig. 3 FESEM images of the Cu_2O crystals with different *R*, (A) 4, (B) 5 and (C) 6.

Table 1 Total interaction energy between OH^- ions and (100), (111) and (110) facets of Cu_2O crystals

Cu_2O facets	(100)	(111)	(110)
E_{ads} (kcal mol^{-1})	−599.792	−618.074	−654.707

To further investigate the evolution of Cu_2O crystals, a series of experiments were conducted to study the shape evolution of the Cu_2O crystals by progressively adjusting the values of *R* from 6.5 to 6.9 (Fig. S1A–E†). It was found that highly monodisperse blurry octahedral structures formed. As a cubic structure, after the Cu_2O cores are formed, new reactants are continuously arriving at the site, Cu_2O has a growth habit of an octahedral morphology enclosed by lowest-energy (111) facets. Furthermore, the {111} faces of these octahedral are arched surfaces in contrast with the planar {111} surfaces, suggesting the morphology of Cu_2O crystals progressively became hexagonal shape.[34] Nanoparticle-aggregated spherical and octahedron-like structures were synthesized, when *R* values were between 4 and 6.9 (Fig. 3 and S1†). It is believed that the reduction in surface energy is the primary driving force for particle-aggregation.[12,22] In addition, the proper reduction rate was obtained at a certain range of pH values, leading to formation of nanoparticle-aggregated spheres and octahedral-like particles.[22]

Remarkably, the appearance of the Cu_2O crystals changed greatly with *R* further increasing from 7 to 10 (Fig. 4). The well-defined hexapods appeared (Fig. 4A–D) exposing 24 {111} facets. Each hexapod had six triangular shaped pods attached at the center and each pod was triangular in shape. The six hexapods were loosely attached at the center. Eight (111) faces were exposed in the twenty four such faces in the case of the hexapod.[25] Moreover, it is noteworthy that the planes {110} disappeared.

Furthermore, when the *R* increases from 7 to 10, the short hexapods represent a progressive structural evolution beyond the octahedral structure with each corner of an octahedron developing into a short square pyramidal branch enclosed by the {111} surfaces. Thus, a structure with 24 {111} facets is formed. The emerged octahedral first-order structures nucleate secondary microcrystals and begin to develop their legs on their six corners along six directions according to the symmetry of the Cu_2O octahedron (Fig. 4). FESEM observation revealed that *R* is a key factor directing the morphology evolution of the Cu_2O nanocrystals. When *R* is 7, it resulted in long-hexapod-shaped Cu_2O crystals (Fig. 4A). In comparison with Fig. 4A, the major long hexapod- and the minor short-hexapod-shaped Cu_2O crystals were observed (Fig. 4B and C). As shown in Fig. 4D, when *R* is 10, it exhibited short-hexapod shaped Cu_2O crystals as the major shapes, simultaneously, showed a small amount of long hexapod Cu_2O crystals. These results can be viewed as the anisotropic fast growth of the six (100) planes.[36]

For designated-tailoring on {111} facets to synthesize multi-branching architectures, a conventional explanation is diffusion-limited growth, which involves that different growth rates of different facets finally lead to the branch growth. In this growth manner, the preferential growth might play an important role in the formation of multi-pods architectures. The central sites of {111} facets can be heavily covered by the adsorbed molecules and well protected, and the growth rates of these sites become much lower than the growth rates on the edge and apex sites. So the original edges of {111} facets disappear, and new inclined planes can be formed between the centers and apexes.[37]

In addition, branching growth can be elucidated based on the diffusion effect around growing crystal surfaces. The apexes of a polyhedral crystal grow faster than the central part of facets, thus forming branches. Xue have synthesized five Cu_2O

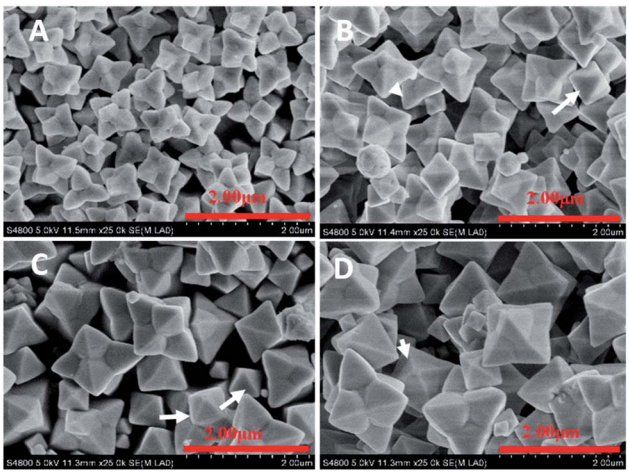

Fig. 4 FESEM images of hexapod Cu_2O crystals with different sizes by controlling the values of *R*, (A) 7, (B) 8, (C) 9 and (D) 10. The white arrow in panel (B and C) represents the occasionally observed short-hexapods, the black arrows in panel (D) display the occasionally observed long-hexapods.

branching growth patterns on the basis of five kinds of polyhedra in the cubic crystal system, including 6-, 8- and 12-pod and 24-pod branching growth patterns.[38–40] In addition, the degree of branching depending on the solution pH has been proved, where high pH favours the branching growth.[41]

These results indicate that the proper reducing ability at a range of pH values plays an important role in the control of crystallization morphologies of Cu_2O, allowing delicate control of the counterbalance between complexation, redox reaction, and pH-dependent precursors.[22]

Crystal structure and chemical compositions of the obtained Cu_2O crystals

The phase composition and structure of these nanocrystals were verified with X-ray diffraction (XRD). Fig. 5A–C give the detailed XRD patterns for a series of the obtained samples. The XRD patterns show the strong and sharp peaks at 2θ = 29.9, 36.5, 42.2, 61.4, and 73.8°, which can be indexed to the (110), (111), (200), (220), and (311) reflection peaks, indicating that all the diffraction peaks are readily indexed to the cubic phase Cu_2O without any impurities, such as metallic copper or cupric oxide. The strong and sharp peaks indicated that the obtained Cu_2O crystals are highly crystalline. Although their XRD patterns appear to be similar due to the random orientation of particles on a substrate, it is worth noting that obvious differences in the intensity ratios for various peaks were observed, giving a support to the above FESEM images. This is because the facets with a slower growth rate will be exposed more on the crystal surface and consequently exhibit relatively stronger diffraction intensity in the corresponding XRD pattern.[42] Furthermore, such variations of the intensity ratio suggest anisotropic growth of these planes during the growing processes.[43] Specially, the ratio of the peak intensity of (220) peak to that of the (200) facet significantly differ between the various particles, suggesting the growing fractions of {110} facets.[15]

The average crystal size of the resulting microcrystals are calculated, as shown in Table S2,† which are according to the Debye–Scherer formula ($D = 0.89\lambda/\beta \cos\theta$, where λ is the X-ray wavelength (1.5418 Å), θ is the Bragg diffraction angle of the peak, and β is the peak width at half maximum).[44]

To determine the chemical compositions of the obtained Cu_2O crystals and to identify the chemical state of Cu in the samples, wide-range and high-resolution XPS spectra were obtained, and only Cu and O were observed in the spectra (Fig. 5D). The emergence of trace C can be attributed to adventitious carbon from the sample fabrication and/or the XPS instrument. The high-resolution individual XPS lines (inset in Fig. 5D) for Cu 2p of Cu_2O crystals (R = 2) showed two peaks of

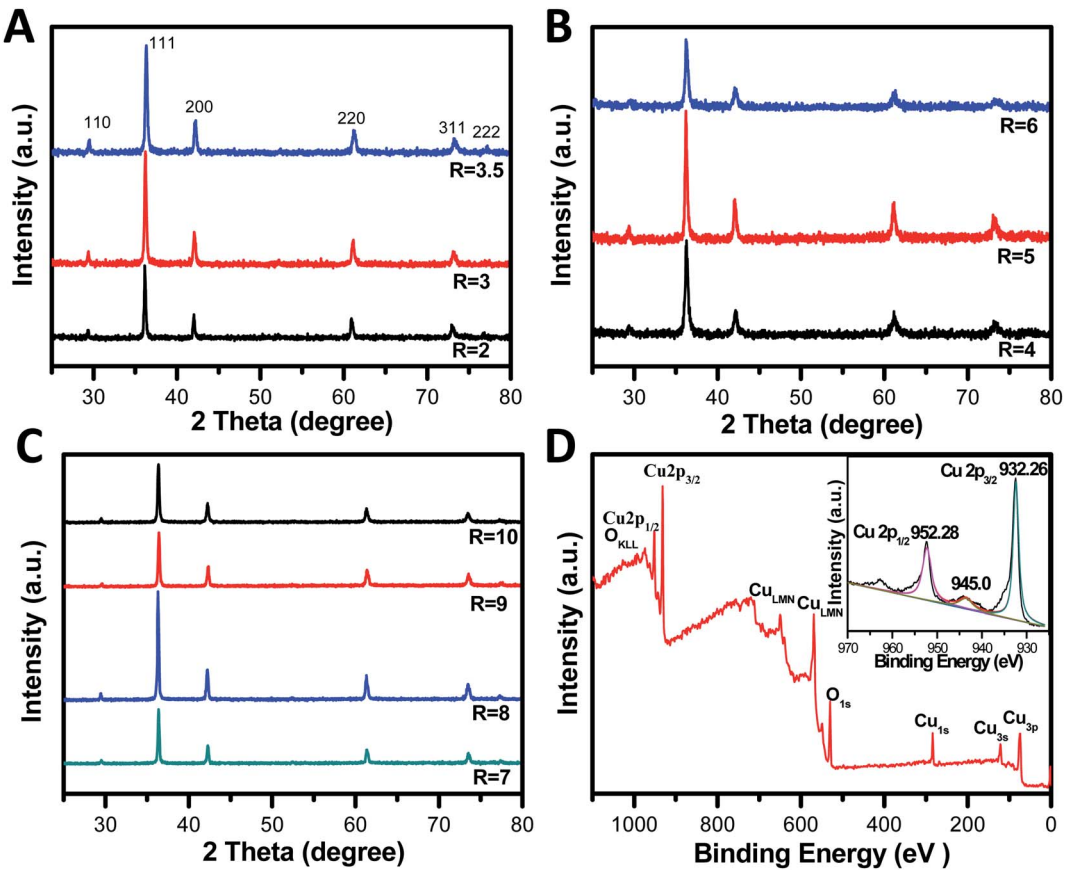

Fig. 5 XRD patterns of different Cu_2O nanocrystals *via* tuning the concentrations of OH^- ions (A–C). XPS spectrum and the high-resolution Cu 2p XPS spectrum of the Cu_2O crystals (R = 2) (inset in D).

932.5 eV and 952.4 eV, and were assigned to Cu $2p_{3/2}$ and Cu $2p_{1/2}$ of Cu^+, respectively, which is in good agreement with the literature reported.[45] The appearance of a satellite peak at 945 eV is due to the transition of the outer electron in Cu^+.[46] Obviously, the XPS results further confirmed Cu_2O was the product and not Cu or CuO,[47,48] which agreed with the XRD results.

Optical properties of RD and hexapod Cu_2O crystals

As is well known, the morphology of Cu_2O crystals significantly influences their physical and chemical properties. The optical absorption behavior as an important fundamental property was investigated by UV-Vis absorption spectrum. The optical properties of RD ($R = 2$) and hexapod ($R = 7$) Cu_2O crystals are shown in Fig. S4A,† all Cu_2O samples display excellent light harvesting capability in the wavelength range of 400–600 nm. Fig. S4B† shows Tauc plots of these Cu_2O crystals with well-defined facets, respectively. As an indirect band gap semiconductor, n should be taken as 2 for Cu_2O,[49] and the calculated band gap energy of RD ($R = 2$) and hexapod ($R = 7$) Cu_2O crystals were measured to be 2.38 and 2.22 eV, respectively. This greater band gap value, as compared to that of bulk Cu_2O at 2.17 eV, is attributed to quantum confinement effects.[50] The observed slight differences in their band-gap values could be attributed for their different morphologies and size as reported in the literature.[51]

Conclusions

In summary, Cu_2O crystals with various shapes including rhombic dodecahedron, to a sphere, octahedron-like and hexapod were systematically synthesized *via* the reduction of copper ions by hydroxylamine hydrochloride in the presence of NaOH. A clear morphological evolution was observed by increasing the NaOH concentration. Furthermore, DFT possibly explained that OH^- ions can selectively adsorb onto the positively charge facets, which facilitate better understanding of the directions of crystal growth. Specifically, at low OH^- ions concentrations (R = 2 and 3), the obtained samples with exposed 12 well-defined high-energy {110} planes possess perfect and regular rhombic dodecahedral morphology with the average diameters of 0.48 and 0.45 μm, respectively. At a higher NaOH concentration (R values ranged from 7 to 10), hexapod-shaped Cu_2O crystals arrived. Thus, the concentration of OH^- ions play an important role in the variation in the morphologies and sizes of the Cu_2O crystals.

Conflicts of interest

There are no conflicts to declare.

Acknowledgements

We thank the Chinese Characters of Shanghai Agricultural Sciences (2018) No. 3-3, National Natural Science Foundation of China (21975279).

Notes and references

1 Z. G. Liu, Y. F. Sun, W. K. Chen, Y. Kong, Z. Jin, X. Chen, X. Zheng, J. H. Liu, X. J. Huang and S. H. Yu, *Small*, 2015, **11**, 2493–2498.
2 X. Liang, L. Gao, S. Yang and J. Sun, *Adv. Mater.*, 2009, **21**, 2068–2071.
3 C. J. Munro, E. C. Bell, M. O. Olagunju, J. L. Cohn, E. M. Zahran, L. G. Bachas and M. R. Knecht, *ACS Sustainable Chem. Eng.*, 2019, **7**, 17055–17064.
4 S. Thoka, A. T. Lee and M. H. Huang, *ACS Sustainable Chem. Eng.*, 2019, **7**, 10467–10476.
5 W. Zhao, W. Fu, H. Yang, C. Tian, R. Ge, C. Wang, Z. Liu, Y. Zhang, M. Li and Y. Lia, *Appl. Surf. Sci.*, 2010, **256**, 2269–2275.
6 P. Cendula, M. T. Mayer, J. Luo and M. Grätzel, *Sustainable Energy Fuels*, 2019, **3**, 2633–2641.
7 X. Yang, S. Zhang, L. Zhang, B. Zhang and T. Ren, *Eur. J. Inorg. Chem.*, 2020, **2020**, 613–616.
8 N. Wang, Y. Zhou, K. Chen, T. Wang, P. Sun, C. Wang, X. Chuai, S. Zhang, X. Liu and G. Lu, *Sens. Actuators, B*, 2021, **333**, 129540.
9 S. Jiao, L. Xu, K. Jiang and D. Xu, *Adv. Mater.*, 2006, **18**, 1174–1177.
10 Y. J. Lee, S. Kim, S. H. Park, H. Park and Y. D. Huh, *Mater. Lett.*, 2011, **65**, 818–820.
11 S. Thoka, A. T. Lee and M. H. Huang, *ACS Sustainable Chem. Eng.*, 2019, **7**, 10467–10476.
12 H. Xu, W. Wang and W. Zhu, *J. Phys. Chem. B*, 2006, **110**, 13829–13834.
13 Y. Dong, F. Tao, L. Wang, M. Lan, J. Zhang and T. Hong, *RSC Adv.*, 2020, **10**, 22387–22396.
14 S. Ghosh, R. Das and M. K. Naskar, *Mater. Lett.*, 2016, **183**, 325–328.
15 X. Yang, S. Zhang, L. Zhang, B. Zhang and T. Ren, *RSC Adv.*, 2019, **9**, 36831–36837.
16 B. Zhang, S. Liao, W. Wu, H. Li and T. Ren, *Phys. Chem. Chem. Phys.*, 2018, **20**, 20117–20123.
17 B. E. Yeo, Y. S. Cho and Y. D. Huh, *CrystEngComm*, 2017, **19**, 1627–1632.
18 L. Tang, J. Lv, S. Sun, X. Zhang, C. Kong, X. Song and Z. Yang, *New J. Chem.*, 2014, **38**, 4656–4660.
19 C. H. Kuo and M. H. Huang, *J. Phys. Chem. C*, 2008, **112**, 18355–18360.
20 A. T. Hagler and C. S. Ewig, *Comput. Phys. Commun.*, 1994, **84**, 131–155.
21 *Materials Studio V7.0*, Accelrys Software Inc. Copyright © 2013, www.accelrys.com.
22 K. Chen and D. Xue, *CrystEngComm*, 2012, **14**, 8068–8075.
23 C. H. Kuo and M. H. Huang, *J. Am. Chem. Soc.*, 2008, **130**, 12815–12820.
24 Y. H. Tsai, C. Y. Chiu and M. H. Huang, *J. Phys. Chem. C*, 2013, **117**, 24611–24617.
25 W. C. Huang, L. M. Lyu, Y. C. Yang and M. H. Huang, *J. Am. Chem. Soc.*, 2012, **134**, 1261–1267.
26 Y. Shang and L. Guo, *Adv. Sci.*, 2015, **2**, 1500140–1500162.

27 Y. Shang, D. Sun, Y. M. Shao, D. F. Zhang, L. Guo and S. H. Yang, *Chem.–Eur. J.*, 2012, **18**, 14261–14266.
28 K. Chanda, S. Rej and M. H. Huang, *Nanoscale*, 2013, **5**, 12494–12501.
29 X. Wang, C. Liu, B. J. Zheng, Y. Q. Jiang, L. Zhang, Z. X. Xie and L. S. Zheng, *J. Mater. Chem. A*, 2013, **1**, 282–287.
30 Y. Zhang, B. Deng, T. R. Zhang, D. M. Gao and A. W. Xu, *J. Phys. Chem. C*, 2010, **114**, 5073–5079.
31 M. H. Huang and P. H. Lin, *Adv. Funct. Mater.*, 2012, **22**, 14–24.
32 J. H. Zhong, G. R. Li, Z. L. Wang, Y. N. Ou and Y. X. Tong, *Inorg. Chem.*, 2011, **50**, 757–763.
33 A. Radi, D. Pradhan, Y. Sohn and K. T. Leung, *ACS Nano*, 2010, **4**, 1553–1560.
34 J. Y. Ho and M. H. Huang, *J. Phys. Chem. C*, 2009, **113**, 14159–14164.
35 M. Leng, C. Yu and C. Wang, *CrystEngComm*, 2012, **14**, 8454–8461.
36 K. Chen, C. Sun, S. Song and D. Xue, *CrystEngComm*, 2014, **16**, 5257–5267.
37 S. Sun, H. You, C. Kong, X. Song, B. Ding and Z. Yang, *CrystEngComm*, 2011, **13**, 2837–2840.
38 J. Xu and D. Xue, *Acta Mater.*, 2007, **55**, 2397–2406.
39 X. Zhao, X. Ren, C. Sun, X. Zhang, Y. Si, C. Yan, J. Xu and D. Xue, *Funct. Mater. Lett.*, 2008, **1**, 167–172.
40 X. Zhao, Z. Bao, C. Sun and D. Xue, *J. Cryst. Growth*, 2009, **311**, 711–715.
41 K. Chen, Y. Si and D. Xue, *Nanosci. Nanotechnol. Lett.*, 2011, **3**, 423–428.
42 Y. Xiong and Y. Xia, *Adv. Mater.*, 2003, **19**, 3385–3391.
43 Y. Sui, W. Fu, H. Yang, Y. Zeng, Y. Zhang, Q. Zhao, Y. Li, X. Zhou, Y. Leng, M. Li and G. Zou, *Cryst. Growth Des.*, 2010, **10**, 99–108.
44 X. Zhou, J. Y. Liu, C. Wang, P. Sun, X. L. Hu, X. W. Li, K. Shimanoe, N. Yamazoe and G. Lu, *Sens. Actuators, B*, 2015, **206**, 577–583.
45 L. Pan, J. J. Zou, T. Zhang, S. B. Wang, Z. Li, L. Wang and X. W. Zhang, *J. Phys. Chem. C*, 2013, **118**, 16335–16343.
46 J. Xiong, Z. Li, J. Chen, S. Zhang, L. Wang and S. Dou, *ACS Appl. Mater. Interfaces*, 2014, **6**, 15716–15725.
47 A. Singhal, M. R. Pai, R. Rao, K. T. Pillai, I. Lieberwirth and A. K. Tyagi, *Eur. J. Inorg. Chem.*, 2013, **2013**, 2640–2651.
48 K. Giannousi, G. Sarafidis, S. Mourdikoudis, A. Pantazaki and C. Dendrinou-Samara, *Inorg. Chem.*, 2014, **53**, 9657–9666.
49 W. B. Yu, Z. Y. Hu, M. Yi, S. Z. Huang, D. S. Chen, J. Jin, Y. Li, G. V. Tendeloo and B. L. Su, *RSC Adv.*, 2016, **6**, 97129–97136.
50 C. H. Kuo and M. H. Huang, *J. Phys. Chem. C*, 2008, **12**, 18355–18360.
51 Y. Chang, J. J. Teo and H. C. Zeng, *Langmuir*, 2005, **21**, 1074–1079.